



**Deleterious Effects of Non-framework Al Species on the  
Catalytic Performance of ZSM-5 Crystals Synthesized at Low  
Temperature**

Journal:	<i>Reaction Chemistry &amp; Engineering</i>
Manuscript ID	RE-ART-06-2019-000231.R1
Article Type:	Paper
Date Submitted by the Author:	19-Jul-2019
Complete List of Authors:	Qin, Wei; University of Houston, Chemical and Biomolecular Engineering Zhou, Yunwen; University of Houston, Chemical and Biomolecular Engineering Rimer, Jeffrey; University of Houston, Chemical and Biomolecular Engineering

# Deleterious Effects of Non-framework Al Species on the Catalytic Performance of ZSM-5 Crystals Synthesized at Low Temperature

*Wei Qin, Yunwen Zhou, and Jeffrey D. Rimer\**

Department of Chemical and Biomolecular Engineering, University of Houston, 4726 Calhoun Road, Houston, TX 77204 USA

\* Correspondence sent to: [jdrimer@central.uh.edu](mailto:jdrimer@central.uh.edu)

**Keywords:** zeolite, MFI, ZSM-5, MTH reaction, aluminum coordination, catalyst defects

**Abstract.** ZSM-5 is one of the most widely studied and commercially relevant zeolites. It is also one of the few zeolites that can be synthesized in an all-silica form (silicalite-1), and thus serves as a prototype for mechanistic studies of zeolite crystallization. The MFI framework of ZSM-5 is amenable to a broad range of synthesis conditions, which has led to numerous discoveries of materials with unique physicochemical properties. The exceptional performance of ZSM-5 among zeolite catalysts, coupled with its facile synthesis, has given rise to its widespread use in industrial applications. In this study we highlight the challenges associated with synthesizing ZSM-5 at low temperature (ca. 100°C), which is often necessary to generate small crystals (< 200 nm) with an appreciable quantity of acid sites (i.e. Si/Al < 25). We focus on the incorporation of non-framework Al, which includes extra-framework (octahedral) Al and penta-coordinated Al, as well as Al zoning – a common phenomenon where the density of Al sites within the framework is more prevalent at the outer rim and exterior surfaces of ZSM-5 crystals. We show that synthesis at low temperature, and most notably in growth mixtures containing high aluminum concentration, results in the incomplete incorporation of Al into the ZSM-5 framework that can be partially removed through post-synthesis mild acid treatment. We also show that higher synthesis temperature (170°C) facilitates the incorporation of framework Al; however, in all cases the catalysts prepared in this study exhibit relatively low activity owing in part to the presence of Al defects. The library of ZSM-5 catalysts prepared herein are characterized using methanol to hydrocarbons as a benchmark reaction to assess the performance of various as-made and acid treated samples. Our findings suggest that ZSM-5 may be more difficult to synthesize than is commonly perceived, most notably when examining the various types of defects in crystalline products over a wide range of synthesis conditions.

## 1. INTRODUCTION

The widespread use of zeolites as heterogeneous catalysts in industrial applications is attributed to their exceptionally high (hydro)thermal stability, tunable Brønsted acidity, and unique microporous topologies.<sup>1-3</sup> The incorporation of tetrahedral aluminum in the zeolite framework creates a negative charge that is counterbalanced by an extra-framework cation (e.g. Brønsted acid site in catalysis). The network of one- to three-dimensional micropores in zeolites also provides confined regions for enhanced shape selectivity, and/or specific environments that direct the formation of certain products by stabilizing their associated transition state(s).<sup>4-10</sup> One of the challenges associated with zeolite catalysts is their propensity to rapidly deactivate due to internal diffusion limitations that result in coke formation. This is particularly problematic for small-pore zeolites ( $< 4 \text{ \AA}$  pore apertures), and has led to significant efforts to design nano-sized zeolitic materials with markedly reduced internal diffusion path length.<sup>11-14</sup> There have been many notable advancements in the area of crystal engineering that have led to ultrasmall zeolites,<sup>15-17</sup> 2-dimensional materials,<sup>18-22</sup> hierarchical zeolites,<sup>23-27</sup> and other types of unique architectures that have proven to be effective in reducing transport limitations and improving the overall performance of zeolite catalysts.<sup>28-30</sup>

In select cases, a facile approach to prepare nano-sized zeolites is the judicious adjustment of synthesis parameters, which include (but are not limited to) gel composition, the source of reagents, and temperature. For example, the selection of silicon and/or aluminum sources can have a notable impact on the kinetics of crystallization.<sup>31</sup> Moreover, the intimate contact between these sources and alkali metals, which often serve as structure-directing agents, can dramatically alter crystal growth as well as the final physicochemical properties of zeolites.<sup>32</sup> Among various synthesis parameters, temperature is one that can have a notable impact on particle size. In particular, it is widely reported that low-temperature syntheses favor nucleation over crystal growth, thereby leading to an increase in the number of crystals with a concomitant reduction in average crystal size.<sup>33</sup> Examples include the work of Valtchev and coworkers<sup>34</sup> who systematically examined the effect of temperature on zeolite A (LTA) crystallization and observed a monotonic decrease in crystal size with decreasing synthesis temperature. Rodríguez and coworkers<sup>35</sup> showed for the case of

ZSM-5 (MFI) synthesis that ultrasmall crystals (10–20 nm) could be generated at low temperatures (70–90 °C).

Numerous studies of ZSM-5 size control can be found in the literature where the vast majority of cases examine the formation of nano-sized crystals with relatively low aluminum content (i.e. Si/Al > 25). In catalytic reactions, it is often desirable to prepare ZSM-5 with a high acid density; however, it is nontrivial to synthesize ZSM-5 with the dual conditions of high Al content and small crystal size. Reported studies in literature where this scenario is achieved tend to involve nano-sized ZSM-5 synthesis at low temperature.<sup>36</sup> One potential pitfall of low temperature conditions is a greater probability of sacrificing the percent crystallinity of the final product, particularly when synthesizing materials within a reasonable time period (i.e. on the order of hours or days). Valtchev and coworkers<sup>37</sup> recently reported the synthesis of ZSM-5 at 100 °C leading to crystal sizes of 100 – 150 nm and Si/Al ratios of 25 to 35. Their study revealed that lower temperature resulted in less crystalline ZSM-5 (i.e. reduced framework Al) and a higher percentage of amorphous (extra-framework) species and defects (e.g. silanol nests).

In this study, we focus on the deleterious effect of ZSM-5 synthesis at low temperature, and the challenges associated with achieving Al-rich (Si/Al < 25) nanomaterials for applications in catalysis. Using a combination of experimental techniques, including <sup>29</sup>Al MAS NMR, we show that low temperature favors the incorporation of non-framework Al. These species include extra-framework (octahedral) Al as well as penta-coordinated Al. Moreover, the ZSM-5 catalysts prepared under these conditions are susceptible to Al zoning, which is a well-known phenomenon in zeolite synthesis (most notably for ZSM-5)<sup>38, 39</sup> where a disproportionate number of Al sites in the exterior rim of the crystals leads to a spatial gradient in acid site density. The formation of Al-zoned zeolites could be due to a delayed incorporation of Al into the zeolite during crystallization, as was demonstrated by Padovan et al.<sup>40</sup>; however, some Al-zoned ZSM-5 crystals exhibit a relatively sharp boundary in Si/Al ratio between the exterior Al-rich rim and the interior Si-rich core, which has been explained by the deposition of Al on zeolite surfaces at the end of synthesis (i.e. thermal quenching).<sup>38</sup> Analysis of Al speciation by solid state NMR reveals that many of the Al species associated with low-temperature synthesis of ZSM-5 are not fully incorporated within the zeolite

framework. Typical methods of dealumination include steam and acid treatments.<sup>41-47</sup> Mild applications of the latter are used in this study to remove extra-framework Al. Herein, we examine a series of as-made and acid-treated ZSM-5 materials that were prepared with a range of sol gel Si/Al ratios at low temperature (100°C). Our findings highlight the difficulty of synthesizing “defect-free” ZSM-5 crystals, and the impact of non-framework Al species on the methanol to hydrocarbons (MTH) reaction, which was used as a benchmark to compare the performance of various H-ZSM-5 catalysts.

## 2. EXPERIMENTAL SECTION

**2.1. Materials.** The following reagents were purchased from Sigma-Aldrich: tetraethylorthosilicate (TEOS, 98%), aluminum isopropoxide (AIP, 98%), sodium hydroxide (NaOH, 98%), hydrochloric acid solution (HCl, 1 N), and silica gel (Davisil Grade 636, 35-60 mesh size). Tetrapropylammonium hydroxide (TPAOH, 40%) and sodium aluminate (technical grade) were purchased from Alfa Aesar. Deionized (DI) water was produced with an Aqua Solutions RODI-C-12A purification system (18.2 MΩ). All reagents were used as received without further purification. For reaction studies, methanol was purchased from J.T. Baker (99.8%) and the argon, oxygen, and nitrogen gases were purchased from Praxair with UHP grade (99.999%).

**2.2. Zeolite crystallization.** ZSM-5 zeolites (gel Si/Al = 20, 30, 50, 75, and 100) were synthesized according to a reported protocol [R] using growth solutions with a nominal molar composition of 6 TPAOH:0.1x Na<sub>2</sub>O:25 SiO<sub>2</sub>:0.25x Al<sub>2</sub>O<sub>3</sub>:480 H<sub>2</sub>O:100 EtOH, where  $x = 0.5, 0.67, 1.0, 1.67, \text{ or } 2.5$ . TEOS was added to a solution of TPAOH, NaOH and DI water. The mixture was aged at room temperature for 24 h under continuous stirring. AIP was added and the mixture was aged for an additional 24 h at room temperature. The growth solution was then placed in a Teflon-lined stainless steel acid digestion bomb (Parr Instruments) and heated at either 100 or 170°C under autogenous pressure for 3 days. The solution was then removed from the oven and immediately cooled to room temperature. The preparation of ZSM-5 with gel Si/Al = 22 (sample Z22-2) was performed according to a protocol reported by Palčić et al.<sup>37</sup> whereby sodium aluminate and TPAOH were combined in DI water with continuous stirring until the solution was

clear. To this mixture was added TEOS to yield a molar composition of 1.23 Na<sub>2</sub>O:9.74 TPAOH:1.0 Al<sub>2</sub>O<sub>3</sub>:43.2 SiO<sub>2</sub>:806 H<sub>2</sub>O. This growth mixture was aged at 80°C for 24 h, and then placed in an acid digestion bomb and heated at 100°C for 7 days. This same procedure was repeated to prepare sample Z22-1 with identical molar composition using a different Al source (AIP), room temperature aging for 24 h, and heating at 100°C for 3 days.

Solid products were isolated from the supernatant by three cycles of centrifugation (13,000 rpm) and washing, and then dried in air under ambient conditions. A fraction of the synthesized ZSM-5 samples were acid treated in 0.1 M HCl (3 g sample per 100 g of solution) at room temperature for 5 h. After drying, both the treated and untreated samples were calcined in flowing dried air (100 mL min<sup>-1</sup>, Matheson Tri-Gas) at 550°C (using heating and cooling rates of 1 °C min<sup>-1</sup>) for 5 h to removed occluded organic structure-directing agent. To prepare catalysts, ion-exchange was performed three times using a 1 M NH<sub>4</sub>NO<sub>3</sub> solution containing 2 wt% of calcined zeolite samples, which was heated at 80°C under continuous stirring for 2 h. The exchanged samples were dried and calcined again to obtain protonated (H-form) zeolites.

**2.3. Materials characterization.** Powder X-ray diffraction (XRD) patterns were collected on a Rigaku diffractometer using Cu K $\alpha$  radiation (40kV, 40 mA). Scanning electron microscopy (SEM) was conducted at the Methodist Hospital Research Institute in the Department of Nanomedicine SEM Core using a Nova NanoSEM 230 instrument with ultrahigh resolution FESEM (operated at 15 kV and a 5mm working distance). Energy dispersive X-ray spectroscopy (EDX) was performed using a JEOL SM-31010/METEK EDAX system at 15 kV and 15 mm working distance. X-ray photoelectron spectroscopy (XPS) analysis of samples was performed using a PHI 5800 ESCA (Physical Electronics) multitechnique system equipped with a standard achromatic Al K $\alpha$  X-ray source (1486.6 eV) operating at 300 W (15 kV and 20 mA) and a concentric hemispherical analyzer. The equipment neutralizer component was utilized to prevent charging effects. All data were collected at a 45° takeoff angle. Solid-state NMR experiments were performed at 11.7 T on a JEOL ECA-500 spectrometer, equipped with a 3.2mm Field Gradient Magic Angle Spinning Probe. <sup>27</sup>Al MAS NMR spectra were obtained at a spinning frequency of 12.5 kHz, pulse of  $\pi/12$ , relaxation

delay of 0.8 s and 4 k scans. The  $^{27}\text{Al}$  chemical shift was referenced using 1M  $\text{Al}(\text{NO}_3)_3$  aqueous solution. The BET surface area was measured by  $\text{N}_2$  adsorption using a Micromeritics ASAP2020 instrument.

**2.4. Reaction testing.** Methanol-to-hydrocarbon (MTH) reaction was carried out in a  $\frac{1}{4}$  inch stainless steel tube installed in a Thermo Scientific Lindberg Blue M furnace. All catalysts beds of ZSM-5 (36.9 mg, 40-60 mesh size) were mixed with silica gel (113.1 mg, 35-60 mesh size) and held between two plugs of quartz wool. A K-type thermocouple (Omega Engineering) was inserted into the stainless tube to measure the temperature of the catalyst bed. Prior to the reaction, the catalyst bed was pretreated *in situ* at  $550^\circ\text{C}$  for 3 h under flow of dried air ( $6\text{ cm}^3\text{ min}^{-1}$  of  $\text{O}_2$ ,  $24\text{ cm}^3\text{ min}^{-1}$  of  $\text{N}_2$ ). The catalyst bed was then cooled to the reaction temperature,  $350^\circ\text{C}$ . Methanol was fed by a syringe pump (Harvard Apparatus) at  $7\text{ }\mu\text{L min}^{-1}$  into a heated inert gas stream of Ar (Matheson,  $30\text{ cm}^3\text{ min}^{-1}$ ), which resulted in a reactant flow with a weight hourly space velocity (WHSV) of  $9\text{ h}^{-1}$ . Reaction effluent was evaluated using an on-stream gas chromatograph (Agilent 7890B) equipped with a FID detector and an Agilent DB-1 capillary column. Methanol and dimethyl ether (DME) are considered as reactant with the conversion ( $X$ ) defined as

$$X = [1 - C_{eff}/C_{feed}] \times 100\% \quad (1)$$

where  $C_{eff}$  is the concentration of both methanol and DME in the effluent and  $C_{feed}$  is the concentration of methanol in the feed. The selectivity ( $S_i$ ) of hydrocarbon product  $i$  is defined as

$$S_i = [C_i/C_{t,eff}] \times 100\% \quad (2)$$

where  $C_i$  is the concentration of hydrocarbon  $i$  in the effluent and  $C_{t,eff}$  is the total concentration of hydrocarbons in the effluent.

### 3. RESULTS AND DISCUSSION

**3.1. ZSM-5 synthesis with varied sol gel Si/Al ratio.** The protocol for ZSM-5 (MFI) synthesis was adapted from a previous study by Persson and workers<sup>48</sup> that reported nano-sized (ca. 150 nm) crystals prepared at low synthesis temperature ( $100^\circ\text{C}$ ). As previously noted, low temperature is commonly used to produce small ZSM-5 crystallites.<sup>33, 35, 49</sup> One of the objectives of this study was to assess the degree to

which the nominal aluminum content of the crystalline product could be varied. For instance, Persson et al. expressed difficulties with incorporating additional Al into ZSM-5 beyond their reported value of Si/Al = 50. This is consistent with a broader survey of literature wherein it is difficult to find reports of ultrasmall ZSM-5 crystals (<200 nm) prepared with high Al content (i.e. Si/Al  $\leq$  25).

Here, we examined Al incorporation by adjusting the sol gel Si/Al ratio at a fixed synthesis temperature of 100°C. All zeolite samples are denoted using the nomenclature ZX, where Z is in reference to ZSM-5 and X is the sol gel Si/Al ratio. We varied X from 20 to 100 (Table 1) by adjusting the quantity of aluminum source while keeping the silica content fixed. Aluminum incorporation into the zeolite framework requires a structure-directing agent (SDA) to facilitate the formation of the 3-dimensional porous network, and also to compensate the negative charge of tetrahedral Al sites within the MFI framework. To this end, we used a combination of tetrapropylammonium (TPA<sup>+</sup>) and Na<sup>+</sup> ions as organic and inorganic SDAs, respectively. For each synthesis, we adjusted the NaOH content in order to maintain a constant sodium-to-aluminum (Na<sup>+</sup>/Al) ratio. Powder X-ray diffraction (XRD) patterns of as-made ZSM-5 samples (Figure S1) confirm that syntheses with X  $\geq$  30 result in ZSM-5 without noticeable impurities or residual amorphous material, whereas higher Al content (X = 20) leads to an amorphous product. The latter can be avoided when using higher Na<sup>+</sup> concentration, analogous to protocols in literature,<sup>37</sup> which leads to a crystalline product (sample Z22-1). Although there is no apparent amorphous peak in its powder XRD pattern (Figure S1), it is evident that sample Z22-1 is not fully crystalline by virtue of its <sup>27</sup>Al MAS NMR spectrum (Figure S4) revealing an abnormally low framework Al content (Table 1). Indeed, samples with the highest Al content, Z22-1 and Z30, both have <60% framework Al (i.e. as denoted by the  $\delta$  = 55 ppm resonance peak in the NMR spectra); however, longer synthesis time (sample Z22-2) facilitates Al incorporation, as denoted by an increase to >70% framework Al. Textural analysis by nitrogen adsorption/desorption (Figure S2) reveals a monotonic reduction in BET surface area from 547 to 470 m<sup>2</sup>/g with increasing sol gel Si/Al ratio (samples Z30 to Z100), with only minor differences in micropore volume (Table 1). Elemental analysis by energy-dispersive X-ray spectroscopy (EDX) shows a linear increase in the Si/Al ratio of ZSM-5 crystals (spanning from 17 to 57) with increasing sol gel Si/Al ratio. For all as-synthesized samples with sol gel Si/Al  $\geq$  30,

the product yield decreases monotonically with increasing Al content (Figure S3). Moreover, each zeolite (solid) sample contains a disproportionately larger amount of Al compared to the starting synthesis mixture (i.e.  $\text{Si}/\text{Al}_{(\text{gel})} > \text{Si}/\text{Al}_{(\text{solid})}$ ), which is reasonable given the numerous examples in literature where the final composition of the zeolite differs from the starting gel.

**Table 1.** Properties of ZSM-5 samples synthesized from different sol gel Si/Al ratios.

Sample <sup>a</sup>	T (°C)	Si/Al (gel)	Si/Al (solid)		Al content (%) <sup>b</sup>			Textural analysis	
			EDX	XPS	Al (55 ppm)	Al (31 ppm)	Al (0 ppm)	S <sub>BET</sub> (m <sup>2</sup> /g)	V <sub>micro</sub> (cm <sup>3</sup> /g)
Z20 <sup>c</sup>	100	20	----	----	----	----	----	----	----
Z30	100	30	16.8	15.0	58.5	23.8	17.7	547	0.16
Z50	100	50	26.5	19.0	84.5	4.7	10.8	517	0.15
Z75	100	75	39.4	24.0	83.9	3.6	12.5	475	0.14
Z100	100	100	57.4	25.4	88.6	2.7	8.7	470	0.14
Z30T	100	30	45.6	49.8	85.1	3.9	11.0	498	0.14
Z50T	100	50	52.4	65.2	90.7	2.6	6.7	476	0.16
Z75T	100	75	52.6	56.1	85.9	4.5	9.6	475	0.16
Z100T	100	100	54.8	48.4	90.8	2.2	7.1	488	0.16
Z50H	170	50	30.5	20.7	91.4	1.7	6.9	460	0.14
Z50HT	170	50	34.8	25.3	97.1	0.1	2.8	465	0.13
Z22-1 <sup>d</sup>	100	22	24.5	14.1	52.7	26.1	21.2	359	0.12
Z22-2 <sup>e</sup>	100	22	25.4	13.5	70.4	12.4	17.3	435	0.15

(a) Samples nomenclature: Z = ZSM-5, numbers refer to sol gel Si/Al ratio, T = samples treated with mild acid, and H = samples synthesized at higher temperature; (b) Deconvoluted peaks in <sup>27</sup>Al MAS NMR spectra (Figures 4 and S4); (c) Determined to be amorphous from its powder XRD pattern (Figure S1A); (d) Sample Z22-1 was prepared with increased NaOH content (0.73 Na<sub>2</sub>O:26 SiO<sub>2</sub>); (e) Z22-2 was prepared using a modified procedure reported by Palčić et al.<sup>37</sup> where synthesis gels were heated for 7 days compared to 3 days for other samples (see the Experimental section for details).

ZSM-5 samples exhibit a spheroidal morphology with crystal sizes in the range of 100 – 200 nm (Figure 1). There was no apparent change in crystal size with decreasing sol gel Si/Al ratio. Likewise, the crystals all exhibit some degree of surface roughness (Figure 1, inset images), which is reflected in N<sub>2</sub> adsorption/desorption profiles (Figure S2) showing hysteresis at  $P/P_0 > 0.75$  that is attributed to interparticle

porosity. Comparison of SEM images does not indicate a systematic change in surface roughness with Al content. This is seemingly inconsistent with the trend proposed by Stucky and coworkers<sup>50</sup> who reported that rough and smooth ZSM-5 crystals are formed in Al-rich and Al-deficient synthesis gels, respectively. They attributed the rough surface features of ZSM-5 crystals to a branching epitaxial growth of Al-rich MFI nanocrystals near the end of zeolite crystallization due to Al zoning. While spatial gradients in elemental composition of zeolite ZSM-5 are widely reported, the synthesis conditions and processes leading to Al zoning are not well understood.

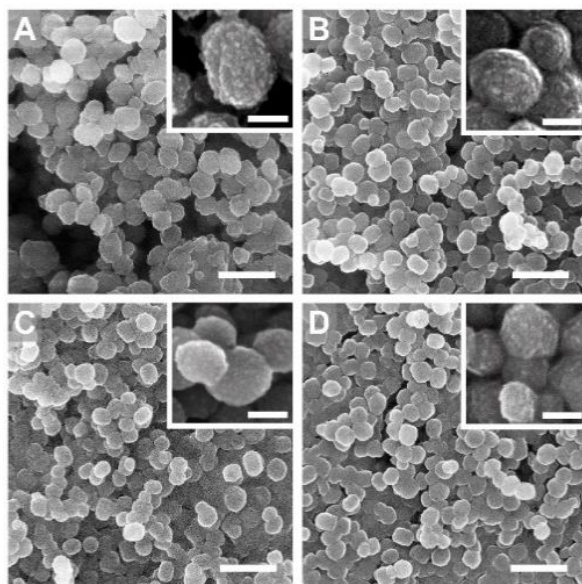


**Figure 1.** Scanning electron micrographs of the following as-made ZSM-5 samples: (A) Z30, (B) Z50, (C) Z75, and (D) Z100. The average size (diameter) of crystals measured from at least 30 particles within a single batch is  $198 \pm 26$  nm,  $182 \pm 15$  nm,  $169 \pm 15$  nm, and  $167 \pm 11$  nm, respectively. Scale bars are equal to 500 nm. Insets are higher magnification images of representative crystals highlighting surface roughness. Scale bars of the insets are equal to 100 nm.

To determine if as-made ZSM-5 samples are Al-zoned, we compared the Si/Al ratios of solids measured by EDX and X-ray photoelectron spectroscopy (XPS). EDX has a sampling depth around two micrometers and was used to obtain the bulk chemical composition of each sample. XPS is a surface-sensitive technique with a sampling depth of only a few nanometers that was used to obtain the surface (or outer rim) chemical

composition. The results of elemental analysis are summarized in Table 1. Interestingly, the sample prepared with the highest quantity of Al (Z30), which also has the highest degree of surface roughness (Figure 1A, inset), exhibits negligible Al zoning. This is a counter example to the correlation reported by Stucky and coworkers linking Al zoning with enhanced surface roughness. We also find that the ZSM-5 sample prepared with the least Al content (Z100) exhibits the highest degree of Al zoning. When comparing the entire series of samples, we observe a linear dependence of the  $Al_{(surface)}/Al_{(bulk)}$  ratio (or the degree of Al zoning) of extracted solids on the sol gel Si/Al ratio (Figure 2A, triangles).

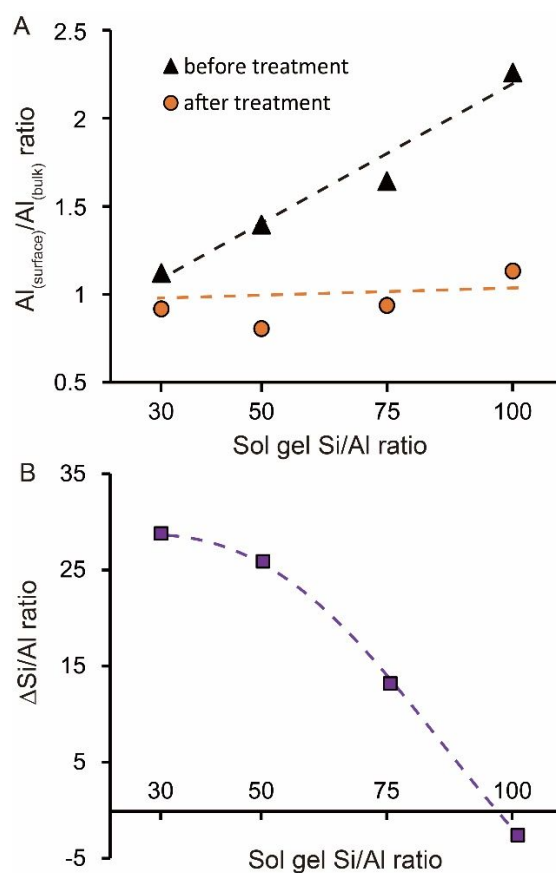


**Figure 2.** (A) Ratio of surface Al content (measured by XPS) and bulk Al content (measured by EDX) after hydrothermal treatment (3d at 100°C) as a function of the sol gel Si/Al ratio of the synthesis mixture. Data are plotted for as-made zeolites before acid treatment (black triangles) and after acid treatment (orange circles). (B) Difference between the Si/Al ratio measured by EDX of zeolite samples before and after acid

treatment as a function of the sol gel Si/Al ratio of the synthesis mixture, where  $\Delta\text{Si/Al ratio} = \text{Si/Al (after acid treatment)} - \text{Si/Al (before acid treatment)}$ . Dashed lines are interpolated to guide the eye.

Prior studies have suggested different types of Al coordination in Al-zoned ZSM-5. For instance, it has been suggested that Al in the exterior rim is crystalline (i.e. framework Al, denoted as *FAl*).<sup>50</sup> Alternatively, it has been posited that Al zoning may be attributed to Al deposition on the zeolite surface during the thermal quenching (cooling) step when solids are extracted from the mother liquor.<sup>38</sup> The latter hypothesis indicates that the formation of an Al-rich exterior could be attributed to extra-framework Al (denoted as *EFAI*). To determine the chemical nature of Al zoning in our ZSM-5 samples, we performed a common method of removing EFAI via mild acid treatment. Notably, as-made zeolites were treated with 0.1 M HCl at room temperature, which is reported to exclusively remove EFAI without extracting FAl.<sup>51, 52</sup> We refer to the acid-treated samples herein as *ZXT* (where *T* = treated). After acid treatment, the physicochemical properties of each sample were evaluated. Mild acid treatment removes Al from the zeolites, resulting in two observed effects. First, acid-treated samples lack any evidence of Al zoning, i.e.  $\text{Al}_{(\text{surface})}/\text{Al}_{(\text{bulk})} \approx 1$  (Figure 2A, circles). As shown in Table 1, we also observe by EDX that irrespective of the original sol gel composition, all Si/Al ratios of acid-treated samples converge to  $\text{Si/Al} \approx 50$  (i.e. the nominal sol gel Si/Al ratio reported by Persson and coworkers<sup>48</sup>). Comparison of EDX and XPS data also reveal negligible Al zoning in all acid-treated samples. Moreover, we observe that the total loss of Al during acid treatment monotonically decreases with increasing sol gel Si/Al (Figure 2B). It should be noted that the most significant reduction in zoning occurs for zeolites with the highest gel Si/Al ratio (Figure 2A, Z100); however, the net change in solid Si/Al for the latter is minimal (Figure 2B) owing to the low quantity of Al used in the synthesis. Conversely, samples with low Si/Al ratio (e.g. Z30) show no evidence of Al zoning, but acid treatment results in the most significant loss of Al and the most notable change in solid Si/Al ratio.

Significant shifts in Al content with acid treatment is evidence for the presence of non-framework Al. In order to gain a better understanding of Al speciation, we used <sup>27</sup>Al MAS NMR to distinguish between framework and extra-framework species. Figure 3 contains the <sup>27</sup>Al MAS NMR spectra of H-ZSM-5 (acid

form) samples prepared with sol gel Si/Al ratios spanning from 30 to 75. The peaks at  $\delta = 55$  and 0 ppm in  $^{27}\text{Al}$  MAS NMR spectra correspond to tetrahedral Al (FAI) and octahedral Al (EFAI), respectively.<sup>45</sup> As previously discussed, samples prepared at higher Al content (e.g. Z30) have  $< 60\%$  FAI, whereas the samples prepared at lower Al content have  $85 \pm 2\%$  FAI (Table 1). NMR spectra also contain peaks around  $\delta = 31$  ppm that increase in relative intensity with higher Al content in the synthesis mixture. This peak has been assigned to penta-coordinated Al and is frequently observed in amorphous aluminosilicates.<sup>53, 54</sup> The flexibility of penta-coordinated Al in zeolite has also been investigated By van Bokhoven and coworkers who demonstrated that for zeolite penta-coordinated Al was converted back into FAI species upon ammonia adsorption.<sup>55</sup> In Table 1 we report the percentages of each Al species estimated from the deconvolution of NMR spectra at resonances  $\delta = 0, 31,$  and  $55$  ppm corresponding to octa-, penta-, and tetra-coordinated Al, respectively. An example of peak deconvolution is shown in Figure 4, while analogous plots for all samples are provided in Figure S4 of the Supporting Information.

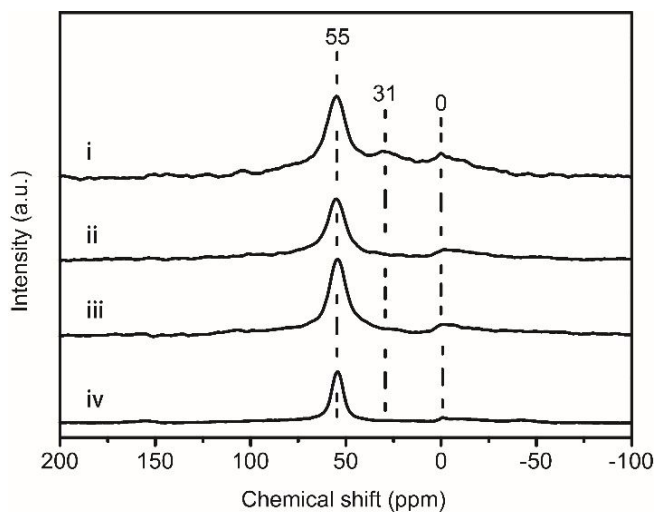


**Figure 3.**  $^{27}\text{Al}$  MAS NMR spectra for the ion-exchanged (H-form) samples (i) Z30, (ii) Z50, (iii) Z75, and (iv) Z100. The spectra are offset along the y-axis for visual clarity. Vertical dashed lines denote peak positions of various Al coordination environments: tetrahedral Al ( $\delta = 55$  ppm), penta-coordinated Al ( $\delta = 31$  ppm), and octahedral Al ( $\delta = 0$  ppm).

The presence of a third Al species in ZSM-5 samples (at  $\delta = 31$  ppm) has long been identified in zeolites and nonporous aluminosilicates<sup>56-60</sup>; however, it is being recognized more frequently in studies of zeolites, although the molecular details of its incorporation within the ZSM-5 framework are not well understood. The Z30 sample has the largest percentage of penta-coordinated Al, but lacks evidence of Al zoning, which suggests the latter is not uniquely correlated with exterior Al species. Indeed, samples with a higher degree of zoning exhibit much less penta-coordinated Al (< 7%), suggesting that EFAl may be responsible for non-framework Al in the outer rim of zeolites. Solid state NMR analysis of the most aluminous H-form sample before (Figure 4A, Z30) and after (Figure 4B, Z30T) acid treatment reveals a significant reduction in the resonance at  $\delta = 31$  ppm with a concomitant reduction in the intensity of the peak at  $\delta = 0$  ppm. The partial removal of EFAl is an expected outcome of mild acid treatment, whereas the nearly complete removal of penta-coordinated Al (or distorted tetrahedral Al) indicates the facile removal of this non-framework species during post-synthesis treatment.

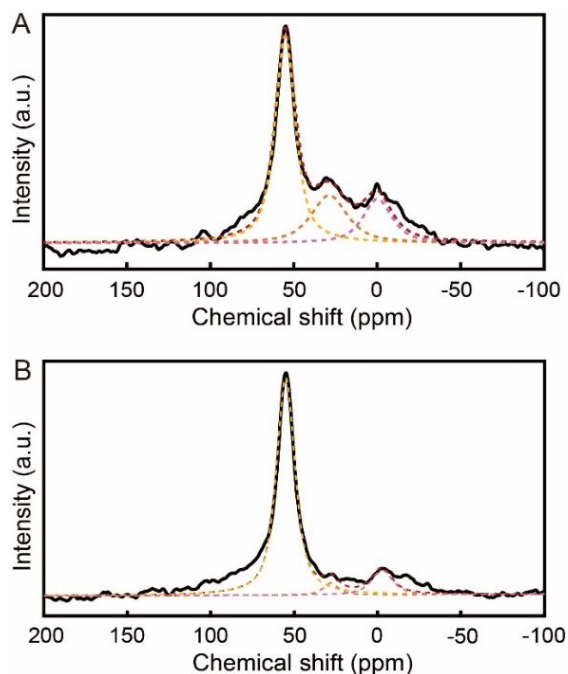


**Figure 4.** Deconvolution of <sup>27</sup>Al MAS NMR spectra showing the curve fittings of two H-form samples: (A) Z30 (as-made aluminous sample) and (B) Z30T (corresponding sample after mild acid treatment). The latter preferentially removes EFAl, but may also lead to the removal of some FAI species.

Here we refer to penta-coordinated Al as non-framework species, placing it in the same category as EFAl. This is consistent with previous studies indicating that signals in the  $^{27}\text{Al}$  MAS NMR spectra around  $\delta = 30$  ppm are extra-framework moieties,<sup>37, 56, 58</sup> whereas resonances at higher chemical shifts (ca.  $\delta = 40$  ppm), which are not observed here, are attributed to less-ordered (or distorted) FAI species.<sup>61</sup> Chen et al.<sup>57</sup> came to a similar conclusion when characterizing dealuminated zeolite omega and showed that distorted tetrahedral Al and penta-coordinated Al are generated by steam treatment at low and high temperatures, respectively. Similar Al speciation was reported by Park et al.<sup>59</sup> when synthesizing a CHA-type  $\text{AlPO}_4$  molecular sieve. Moreover, Pidko et al.<sup>58</sup> investigated the catalytic role of extra-framework Al species in FAU zeolites, introduced by chemical vapor deposition of trimethylaluminum (TMA) followed by its decomposition. Their analysis of these samples by  $^{27}\text{Al}$  MAS NMR identified both penta-coordinated and octahedral Al species in modified FAU catalysts, which collectively resulted in a much higher propane cracking rate than commercial USY zeolite.

**3.2. ZSM-5 synthesis at higher temperature.** The synthesis conditions for Z50 (adopted from literature<sup>48</sup>) were also used in our previous study to generate nano-sized ZSM-5 crystals as seeds for the formation of ZSM-5@silicalite-1 coreshell particles.<sup>62</sup> The epitaxial growth of purely siliceous MFI (silicalite-1) over Z50 seeds was accomplished by first annealing the ZSM-5 particles at high temperature in a slightly supersaturated media to remove any residual amorphous material from the surface of zeolite particles, as well as to remove EFAl (or transform it to FAI). An unreported observation in this study was that ZSM-5 crystals without the high temperature annealing step performed poorly in catalytic studies. Motivated by this observation as well as a general survey of literature showing that ZSM-5 tends to be crystallized at higher temperatures, we investigated Al speciation and zoning in samples that were prepared at a higher synthesis temperature.

There are multiple effects that temperature can impose on zeolite formation, such as altering the solubility of Si and Al sources as well as the crystallization kinetics. It is generally expected that elevated synthesis temperature increases the rate of crystal growth. Moreover, it is anticipated that higher

temperature can facilitate Al incorporation in the MFI framework, thus resulting in a more homogeneous distribution of acid sites. This, in turn, would minimize Al zoning that is the byproduct of Al deposition at later stages of crystallization. To our knowledge, thermodynamic data of aluminosilicate speciation at synthesis conditions (100 – 170°C) is unknown, and thus the premise of a more homogeneous distribution of Al throughout the zeolite particle with increasing temperature is based on a hypothesis that barriers for Si-O-Al bond formation are lowered at these conditions, thus facilitating FAI formation. Beyond temperature, an additional point of concern when preparing ZSM-5 with increased Al content is the molar composition of the starting gel – notably the ratio of Na<sup>+</sup>/Al since Na<sup>+</sup> serves as an inorganic SDA and counterion to negatively-charged FAI sites. Disproportionate ratios leading to an insufficient amount of alkali can hinder Al incorporation. This is a potential reason why the synthesis of Z20 yielded an amorphous product; therefore, to offset the potential negative impact of low inorganic SDA concentration, we performed a similar synthesis (Z22-1) using a growth mixture with increased Na<sup>+</sup> content to promote the nucleation of ZSM-5 with a lower Si/Al ratio (see the Experimental section for details).

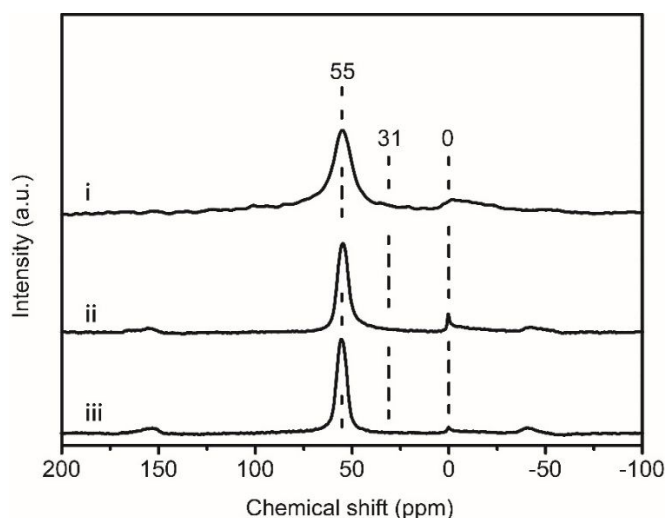


**Figure 5.** <sup>27</sup>Al MAS NMR spectra of H-form zeolites (i) Z50, (ii) Z50H, and (iii) Z50HT. The spectra are offset along the y-axis for visual clarity. Dashed lines highlight peaks corresponding to FAI ( $\delta = 55$  ppm), penta-coordinated Al ( $\delta = 31$  ppm), and EFAI ( $\delta = 0$  ppm).

To test the effect of higher temperature, we repeated the synthesis of Z50 at 170°C (referred to as sample Z50H) and compared its  $^{27}\text{Al}$  MAS NMR spectrum (Figure 5ii) with the corresponding sample after mild acid treatment, Z50HT (Figure 5iii). The higher temperature of ZSM-5 synthesis gives rise to sharper NMR peaks, counter to the broader and more asymmetric peaks of Z50 synthesized at 100°C (Figure 5i). It has been suggested<sup>37</sup> that lower peak intensity for ZSM-5 prepared at low temperature is attributed to so-called *NMR invisible Al species*, which broadens the signal and renders their detection more challenging (particularly for dehydrated Al sites).<sup>63,64</sup> Deconvolution of the NMR data shows that the penta-coordinated Al ( $\delta = 31$  ppm) in Z50H is nearly one-third that of Z50 (Table 1), whereas the quantity of EFAl ( $\delta = 0$  ppm) is reduced by 36% relative to its counterpart prepared at low temperature. Higher synthesis temperature, however, does not fully eliminate non-framework Al from the final product (consistent with previous findings<sup>37</sup>). This is evident when comparing samples before (Z50H) and after (Z50HT) acid treatment, where the latter has the highest fraction of FAI (ca. 97%) and lowest fraction of penta-coordinated Al (ca. 0.1%) among all zeolites analyzed in Table 1. We also observed that higher synthesis temperature does not eliminate Al zoning, but counter to previous samples, acid treatment had little effect on the removal of exterior Al from Z50H, as verified by elemental analysis of samples before and after acid treatment that show no difference in zoning, i.e.  $\text{Al}_{(\text{surface})}/\text{Al}_{(\text{bulk})} \approx 1.4$  for both Z50H and Z50HT.

**3.3. Methanol to hydrocarbons reaction.** Here we compare the catalytic performance of several as-made and acid-treated ZSM-5 samples in the methanol-to-hydrocarbons (MTH) reaction to assess differences in the lifetime and selectivity of catalysts with varying Al speciation and zoning. All zeolites were ion-exchanged to their acid form (HZSM-5) to introduce Brønsted acid sites. The catalysts were tested in a packed bed reactor with a fixed weight hourly space velocity (WHSV) to achieve sub-complete methanol conversion. We first assessed the performance of Z30 (Figure 6, purple triangles), which has high amounts of EFAl and penta-coordinated Al, a low percentage of FAI, and no apparent Al zoning. The initial methanol conversion over this catalyst is relatively low (ca. 18%) and rapidly decreases to ca. 3 % in less than 1 h time on stream (TOS). We next tested the corresponding acid-treated sample, Z30T (Figure 6, red

squares), which resulted in the significant removal of Al, leading to a dramatic increase in FAI (from 59 to 85%), a marked reduction in penta-coordinated Al (from 24 to 4%), and a more moderate reduction in EFAl (from 18 to 11%). The initial methanol conversion over Z30T is 41% and exhibits a slow rate of deactivation with TOS. Interestingly, the performance of Z30T is similar to that of Z75 (Figure 6, yellow circles), which has nearly identical percentages of FAI, EFAl, and penta-coordinated Al as well as similar bulk Si/Al ratios. The primary difference between these two catalysts is that Z75 is slightly Al zoned, yet this does not appear to affect catalyst lifetime, but does have a noticeable impact on selectivity (as discussed below). Indeed, a relatively high percentage of acid sites on exterior surfaces can lead to the loss of shape selectivity owing to the lack of confinement.

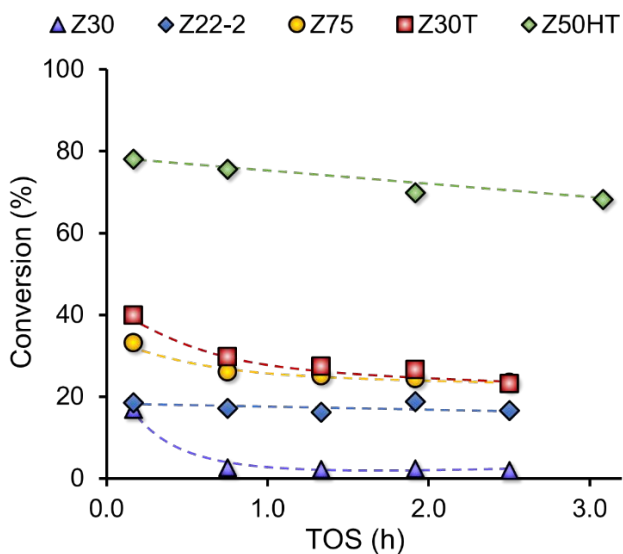


**Figure 6.** Methanol conversion as a function of time-on-stream (TOS) for the following H-form ZSM-5 catalysts: Z30 (purple triangles), Z22-2 (blue diamonds), Z75 (yellow circles), Z30T (red squares), and Z50HT (green diamonds). Each catalyst was synthesized at 100°C, with the exception of H-Z50HT that was prepared at 170°C. Reactions were performed at WHSV = 9 h<sup>-1</sup> and temperature T = 350°C. Dashed lines are interpolated to guide the eye.

Palčić et al. recently reported that Z22-2 with an approximate size of 100 nm exhibits superior MTH performance relative to an industrial ZSM-5 catalyst (1 – 3 μm in size) supplied by Süd-Chemie.<sup>37</sup> The unique properties of Z22-2 were attributed in part to its synthesis at 100°C, which resulted in a 70%

crystalline product with markedly lower Brønsted acidity ( $79 \mu\text{mol g}^{-1}$ ) compared to the commercial catalyst ( $582 \mu\text{mol g}^{-1}$ ). They selected longer contact time (WHSV =  $1 \text{ h}^{-1}$ ) and higher temperature ( $450^\circ\text{C}$ ) for their catalytic tests, which resulted in Z22-2 having a longer lifetime and a 6.3-fold higher propene-to-ethene ratio ( $C_3=C_2$ ) compared to commercial ZSM-5. Here, we performed catalytic testing at a different set of reaction conditions (WHSV =  $9 \text{ h}^{-1}$  and  $350^\circ\text{C}$ ) to ensure sub-complete methanol conversion. As shown in Figure 6, we observe that Z22-2 exhibits a methanol conversion of ca. 20%, nearly identical to Z30 with a much slower rate of deactivation. The lower reaction temperature and shorter contact time used in our experiments likely explain the disparity in catalyst performance. Indeed, the catalysts in Figure 6 that were prepared at low synthesis temperature all exhibit poor activity. It is apparent that the significant quantities of non-framework Al in ZSM-5 synthesized at  $100^\circ\text{C}$  has a negative impact on catalyst performance. Moreover, we show that acid treatment to remove a large percentage of non-framework Al leads to only marginal improvement, suggesting there is something inherently defective in these materials that cannot be easily corrected by post-synthesis treatment. To test this hypothesis, we performed the MTH reaction using the sample prepared at  $170^\circ\text{C}$  after acid treatment, Z50HT (Figure 6, green diamonds). As previously noted, this sample had the highest percentage of FAI and lowest percentages of non-framework Al among all zeolites. As shown in Figure 6, the initial methanol conversion using this catalyst (ca. 80%) is nearly double those of the other catalysts, including Z75 (i.e. a material with approximately the same bulk Si/Al ratio prepared a low temperature). This suggests that higher synthesis temperature produces ZSM-5 crystals with fewer defects; however, beyond the relative amounts of EFAI and penta-coordinated Al, or the degree of Al zoning, it is difficult to elucidate the exact cause of the unexpectedly low activity of all ZSM-5 catalysts.

We also compared MTH selectivities for several ZSM-5 samples prepared at low temperature (Figure 7A). Using the initial time points in Figure 6, we observe subtle differences in the product distribution among all catalysts studied; however, a signature feature of all samples is the relatively high percentage of methane (10 – 20%) in the effluent. We attribute this to the large percentages of non-framework Al species.

For instance, Lercher and coworkers<sup>65-67</sup> have proposed that EFAl promotes the formation of formaldehyde and enhances the aromatics-based cycle of the hydrocarbon pool (HCP) mechanism for MTH reactions.

<sup>68-70</sup> Hwang et al.<sup>71</sup> proposed that formaldehyde and methane are generated

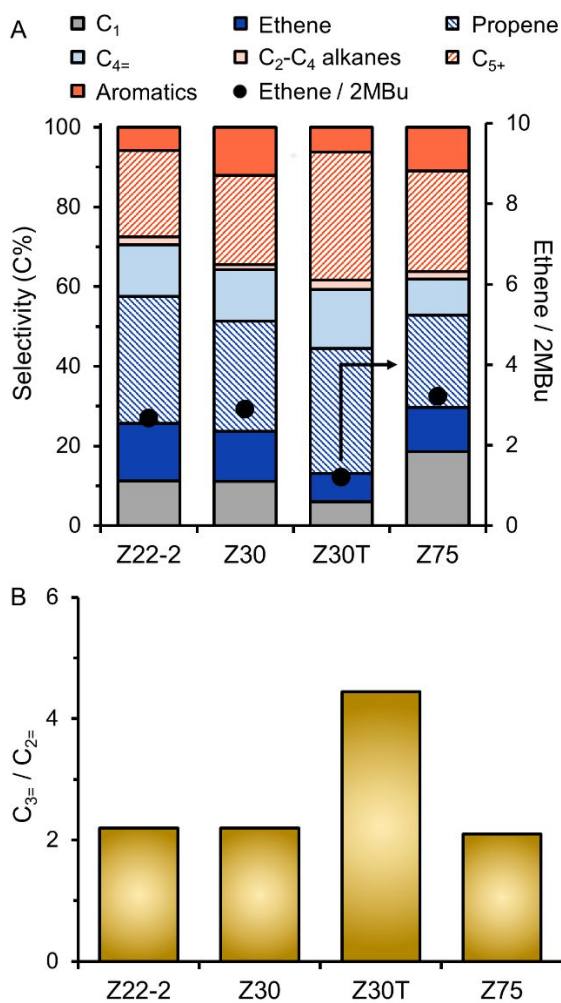


**Figure 7.** (A) Comparison of four H-form ZSM-5 catalysts prepared at low temperature: Z22-2, Z30, Z30T, and Z75. These catalysts exhibit similar initial methanol conversion (20 – 40%). (left axis) Selectivities of each catalyst in MTH reactions at sub-complete methanol conversion (17, 18, 40, and 33%, respectively). (right axis) Corresponding ethene-to-2MBu ratio (black circles) for each catalyst. (B) Comparison of the propene-to-ethene ( $C_{3=}/C_{2=}$ ) ratio for the four catalysts.

simultaneously via methanol disproportionation. Arora et al.<sup>68</sup> investigated the effect of formaldehyde co-feed with methanol on the  $C_{3=}/C_{2=}$  ratio and found that the ratio decreases from 24.7 in the absence of formaldehyde to 0.8 in the case of 20 Pa formaldehyde co-feed, thus indicating the presence of formaldehyde enhances the aromatics cycle. This is consistent with the higher EFAl content of untreated ZSM-5 catalysts, which exhibit relatively low  $C_{3=}/C_{2=}$  ratios (Figure 7B) compared to values for ZSM-5 reported in literature. Comparison of as-made and acid-treated samples reveals a noticeable difference in selectivity. For example, MTH reaction over Z30T (after removal of EFAl by mild acid treatment) leads to a reduction in methane selectivity (ca. 5%). In addition, the acid-treated catalyst exhibits a higher  $C_{3=}/C_{2=}$  ratio (Figure 7B), which indicates the promotion of the olefins-based cycle of the HCP mechanism. Conversely, the lower  $C_{3=}/C_{2=}$  ratios observed for all untreated samples is consistent with EFAl promotion of the aromatic-based cycle of the HCP mechanism. Additional evidence is gleaned from the reduced ethylene-to-2MBu ratio in Figure 7A (where 2-MBu refers to the sum of 2-methylbutane and 2-methyl-2-butene). This ratio is conventionally used in literature as an indicator of the relative propagation of the two cycles in the HCP mechanism.<sup>29, 72</sup>

Brønsted acidity can have a significant effect on product selectivity. This was highlighted in a review by Weckhuysen and coworkers<sup>73</sup> who reported a linear relationship between propene selectivity and Si/Al ratio (or reduced Brønsted acidity). As proof of concept, the same group also reported a study in which they showed that propene yield can be increased as high as 53% over HZSM-5 by reducing Brønsted acid sites via calcium exchange.<sup>74</sup> Another study of MTH over HZSM-5 by Khare et al.<sup>72</sup> found that the ethene-to-2MBu ratio increased from 0.8 to 2.4 with decreasing Si/Al ratio (from 1580 to 55), suggesting that the propagation rate of aromatics-based cycle is enhanced with higher aluminum content. In our study, it is difficult to quantify acidity and assess trends among samples with such large variance in Al speciation. A prior study by Wang et al.<sup>53</sup> characterized proton-exchanged tetrahedral and penta-coordinated Al in amorphous silica-alumina and reported similar Brønsted acidity; however, our data in Figure 7B for as-made samples reveals that relatively large changes in non-framework Al have little impact on the  $C_{3=}/C_{2=}$  ratio. Indeed, samples Z22-2, Z30, and Z75 all have varying quantities of Al species (and bulk Si/Al ratios),

but similar activity and selectivities. The removal of non-framework Al species leads to improved lifetime and higher  $C_{3=}/C_{2=}$  ratio (e.g. sample Z30T); however, it is also evident that the presence of non-framework Al renders such trends among the entire set of samples more convoluted. Indeed, the comparison of ZSM-5 catalysts containing high percentages of octahedral and penta-coordinated Al requires the elucidation of acid strength (relative to FAI sites) and their putative role(s) in the catalytic reaction, which is not well understood and outside the scope of this study.

#### 4. CONCLUSION

In summary, we have demonstrated that the incorporation of Al into ZSM-5 is often incomplete, leading to non-framework sites that result in poor catalytic performance. This is particularly true for low temperature syntheses, which are ostensibly necessary to prepare ZSM-5 materials with small crystal size (i.e. less than 200 nm) and high Al content (i.e.  $Si/Al < 25$ ). Our findings indicate that higher synthesis temperature leads to improved catalyst performance, presumably by facilitating Al incorporation into framework sites; however, the materials prepared at high temperature in this study still possess defects, many of which may not be readily detected using common characterization techniques. In general, comparisons between zeolites of similar physicochemical properties where the synthetic material of choice exhibits inferior catalytic performance to a benchmark material (e.g. commercial catalyst) are rarely reported in literature.

One of the primary intents of this study was to highlight the challenges of ZSM-5 synthesis that often get overlooked – particularly considering it is one of the most synthesized, characterized, tested, and commercially used materials among the ca. 245 known zeolites. While ZSM-5 is arguably much easier to synthesize compared to the vast majority of framework types, this does not necessarily imply the ease of preparing ZSM-5 with few defects. It remains to be determined what set of synthesis conditions either promote or reduce defects in ZSM-5 catalysts. Moreover, the variability in reaction conditions used to assess the performance of ZSM-5 catalysts and the lack of a consistent benchmark make it difficult to draw comparisons among different published studies. This becomes even more critical when trying to develop fundamental structure-performance relationships in zeolite catalysis. In light of the growing impact of data

analytics and machine learning, it would be beneficial to populate databases with information on synthesis failures, which although sparsely available, can be equally important as data on successful syntheses.

The library of ZSM-5 materials synthesized and tested here are a relatively small fraction of examples that highlight the impact of reaction conditions on the generation of defects. In this study, we focus solely on non-framework Al and the phenomenon of zoning; however, it is important to state that there are potentially other factors that contribute to the unexpectedly low activity of these zeolites in MTH reactions. Examples may include (but are not limited to) the blocking of pores, the presence of silanol nests, and/or residual amorphous material that is undetected in powder X-ray diffraction patterns. Moreover, it is evident from a survey of literature that the presence of non-framework Al, under certain circumstances, can have a positive impact on catalyst performance depending on the chemical reaction, zeolite framework type, and reaction conditions (e.g. temperature and space velocity). There is an increasing number of studies that report penta-coordinated Al, although it is not fully understood how these species are incorporated in zeolites and to what extent they influence catalytic performance. Indeed, more detailed experimental and computational investigations are needed to better understand the role of various Al species and their impact (either positive or negative) on catalytic reactions, including techniques to differentiate and quantify the acid strength of penta-coordinated and tetrahedral Al sites.

## ACKNOWLEDGMENTS

We acknowledge financial support primarily from the U.S. Department of Energy, Office of Science, Office of Basic Energy Sciences under Award Number DE-SC0014468. Additional support was provided by the Welch Foundation (Award E-1794).

## REFERENCES

1. Davis, M.E., *Ordered porous materials for emerging applications*. Nature, 2002. **417**: 813.
2. Martínez, C. and A. Corma, *Inorganic molecular sieves: Preparation, modification and industrial application in catalytic processes*. Coordination Chemistry Reviews, 2011. **255**: 1558-1580.
3. Primo, A. and H. Garcia, *Zeolites as catalysts in oil refining*. Chem Soc Rev, 2014. **43**: 7548-7561.

4. Chen, N.Y., T.F. Degnan, and C.M. Smith, *Molecular Transport and Reaction in Zeolites: Design and Application of Shape Selective Catalysis*. 1994: Wiley. 328-328.
5. Degnan, T.F., *The implications of the fundamentals of shape selectivity for the development of catalysts for the petroleum and petrochemical industries*. Journal of Catalysis, 2003. **216**: 32-46.
6. Gounder, R. and E. Iglesia, *The catalytic diversity of zeolites: confinement and solvation effects within voids of molecular dimensions*. Chemical communications (Cambridge, England), 2013. **49**: 3491-509.
7. Gallego, E.M., M.T. Portilla, C. Paris, A. León-Escamilla, M. Boronat, M. Moliner, and A. Corma, "Ab initio" synthesis of zeolites for preestablished catalytic reactions. Science, 2017. **355**: 1051.
8. Li, C., C. Paris, J. Martínez-Triguero, M. Boronat, M. Moliner, and A. Corma, *Synthesis of reaction-adapted zeolites as methanol-to-olefins catalysts with mimics of reaction intermediates as organic structure-directing agents*. Nature Catalysis, 2018. **1**: 547-554.
9. Rimer, J.D., *Rational design of zeolite catalysts*. Nature Catalysis, 2018. **1**: 488-489.
10. Kang, J.H., F.H. Alshafei, S.I. Zones, and M.E. Davis, *Cage-defining Ring: A Molecular Sieve Structural Indicator for Light Olefin Product Distribution from the Methanol-to-Olefins Reaction*. ACS Catalysis, 2019.
11. Lupulescu, A.I., W. Qin, and J.D. Rimer, *Tuning Zeolite Precursor Interactions by Switching the Valence of Polyamine Modifiers*. Langmuir, 2016. **32**: 11888-11898.
12. Olafson, K.N., R. Li, B.G. Alamani, and J.D. Rimer, *Engineering Crystal Modifiers: Bridging Classical and Nonclassical Crystallization*. Chemistry of Materials, 2016. **28**: 8453-8465.
13. Rimer, J.D., A. Chawla, and T.T. Le, *Crystal Engineering for Catalysis*. Annual Review of Chemical and Biomolecular Engineering, 2018. **9**: 283-309.
14. Qin, W., A. Agarwal, M.K. Choudhary, J.C. Palmer, and J.D. Rimer, *Molecular Modifiers Suppress Nonclassical Pathways of Zeolite Crystallization*. Chemistry of Materials, 2019. **31**: 3228-3238.
15. Schmidt, I., C. Madsen, and C.J.H. Jacobsen, *Confined Space Synthesis. A Novel Route to Nanosized Zeolites*. Inorganic Chemistry, 2000. **39**: 2279-2283.
16. Tosheva, L. and V.P. Valtchev, *Nanozeolites: Synthesis, Crystallization Mechanism, and Applications*. Chemistry of Materials, 2005. **17**: 2494-2513.
17. Awala, H., J.-P. Gilson, R. Retoux, P. Boullay, J.-M. Goupil, V. Valtchev, and S. Mintova, *Template-free nanosized faujasite-type zeolites*. Nature Materials, 2015. **14**: 447.
18. Corma, A., V. Fornes, S.B. Pergher, T.L.M. Maesen, and J.G. Buglass, *Delaminated zeolite precursors as selective acidic catalysts*. Nature, 1998. **396**: 353-356.
19. Choi, M., K. Na, J. Kim, Y. Sakamoto, O. Terasaki, and R. Ryoo, *Stable single-unit-cell nanosheets of zeolite MFI as active and long-lived catalysts*. Nature, 2009. **461**: 246-249.
20. Zhang, X., D. Liu, D. Xu, S. Asahina, K.A. Cychosz, K.V. Agrawal, Y.A. Wahedi, A. Bhan, S.A. Hashimi, O. Terasaki, M. Thommes, and M. Tsapatsis, *Synthesis of Self-Pillared Zeolite Nanosheets by Repetitive Branching*. Science, 2012. **336**: 1684-1687.
21. Roth, W.J., P. Nachtigall, R.E. Morris, and J. Čejka, *Two-Dimensional Zeolites: Current Status and Perspectives*. Chemical Reviews, 2014. **114**: 4807-4837.
22. Luo, H.Y., V.K. Michaelis, S. Hodges, R.G. Griffin, and Y. Roman-Leshkov, *One-pot synthesis of MWW zeolite nanosheets using a rationally designed organic structure-directing agent*. Chemical Science, 2015. **6**: 6320-6324.
23. Egeblad, K., C.H. Christensen, M. Kustova, and C.H. Christensen, *Templating Mesoporous Zeolites*. Chemistry of Materials, 2008. **20**: 946-960.
24. Chal, R., C. Gérardin, M. Bulut, and S. van Donk, *Overview and Industrial Assessment of Synthesis Strategies towards Zeolites with Mesopores*. ChemCatChem, 2011. **3**: 67-81.
25. Verboekend, D. and J. Pérez-Ramírez, *Design of hierarchical zeolite catalysts by desilication*. Catalysis Science & Technology, 2011. **1**: 879-890.
26. Serrano, D.P., J.M. Escola, and P. Pizarro, *Synthesis strategies in the search for hierarchical zeolites*. Chemical Society Reviews, 2013. **42**: 4004-4035.

27. Sachse, A., A. Grau-Atienza, E.O. Jardim, N. Linares, M. Thommes, and J. García-Martínez, *Development of Intracrystalline Mesoporosity in Zeolites through Surfactant-Templating*. *Crystal Growth & Design*, 2017. **17**: 4289-4305.
28. Dai, W., G. Wu, L. Li, N. Guan, and M. Hunger, *Mechanisms of the Deactivation of SAPO-34 Materials with Different Crystal Sizes Applied as MTO Catalysts*. *ACS Catalysis*, 2013. **3**: 588-596.
29. Khare, R., D. Millar, and A. Bhan, *A mechanistic basis for the effects of crystallite size on light olefin selectivity in methanol-to-hydrocarbons conversion on MFI*. *Journal of Catalysis*, 2015. **321**: 23-31.
30. Shen, Y., T.T. Le, D. Fu, J.E. Schmidt, M. Filez, B.M. Weckhuysen, and J.D. Rimer, *Deconvoluting the Competing Effects of Zeolite Framework Topology and Diffusion Path Length on Methanol to Hydrocarbons Reaction*. *ACS Catalysis*, 2018. **8**: 11042-11053.
31. Liu, H., G. Liu, X. Zhang, D. Zhao, and L. Wang, *Effects of aluminum sources on synthesis and catalytic performance of b-oriented ZSM-5 coatings*. *Microporous and Mesoporous Materials*, 2017. **244**: 164-170.
32. Li, R., N. Linares, J.G. Sutjianto, A. Chawla, J. Garcia-Martinez, and J.D. Rimer, *Ultrasmall Zeolite L Crystals Prepared from Highly Interdispersed Alkali-Silicate Precursors*. *Angewandte Chemie International Edition*, 2018. **57**: 11283-11288.
33. Valtchev, V. and L. Tosheva, *Porous Nanosized Particles: Preparation, Properties, and Applications*. *Chemical Reviews*, 2013. **113**: 6734-6760.
34. Dimitrov, L., V. Valtchev, D. Nihtianova, and Y. Kalvachev, *Submicrometer Zeolite A Crystals Formation: Low-Temperature Crystallization Versus Vapor Phase Gel Transformation*. *Crystal Growth & Design*, 2011. **11**: 4958-4962.
35. Aguado, J., D.P. Serrano, J.M. Escola, and J.M. Rodríguez, *Low temperature synthesis and properties of ZSM-5 aggregates formed by ultra-small nanocrystals*. *Microporous and Mesoporous Materials*, 2004. **75**: 41-49.
36. Triantafyllidis, K.S., L. Nalbandian, P.N. Trikalitis, A.K. Ladavos, T. Mavromoustakos, and C.P. Nicolaides, *Structural, compositional and acidic characteristics of nanosized amorphous or partially crystalline ZSM-5 zeolite-based materials*. *Microporous and Mesoporous Materials*, 2004. **75**: 89-100.
37. Palčić, A., V.V. Ordonsky, Z. Qin, V. Georgieva, and V. Valtchev, *Tuning Zeolite Properties for a Highly Efficient Synthesis of Propylene from Methanol*. *Chemistry – A European Journal*, 2018. **24**: 13136-13149.
38. Danilina, N., F. Krumeich, S.A. Castelanelli, and J.A. van Bokhoven, *Where Are the Active Sites in Zeolites? Origin of Aluminum Zoning in ZSM-5*. *The Journal of Physical Chemistry C*, 2010. **114**: 6640-6645.
39. Dwyer, J., F.R. Fitch, G. Qin, and J.C. Vickerman, *Study of the surface composition of zeolites by fast atom bombardment mass spectrometry*. *The Journal of Physical Chemistry*, 1982. **86**: 4574-4578.
40. Padovan, M., G. Leofanti, M. Solari, and E. Moretti, *STUDIES ON THE ZSM-5 ZEOLITE FORMATION*. *Zeolites*, 1984. **4**: 295-299.
41. Ong, L.H., M. Dömök, R. Olindo, A.C. van Veen, and J.A. Lercher, *Dealumination of HZSM-5 via steam-treatment*. *Microporous and Mesoporous Materials*, 2012. **164**: 9-20.
42. Sano, T., H. Ikeya, T. Kasuno, Z.B. Wang, Y. Kawakami, and K. Soga, *Influence of Crystallinity of HZSM-5 Zeolite on Its Dealumination Rate*. *Zeolites*, 1997. **19**: 80-86.
43. Sano, T., N. Yamashita, Y. Iwami, K. Takeda, and Y. Kawakami, *Estimation of dealumination rate of ZSM-5 zeolite by adsorption of water vapor*. *Zeolites*, 1996. **16**: 258-264.
44. Prodinger, S., H. Shi, S. Eckstein, J.Z. Hu, M.V. Olarte, D.M. Camaioni, M.A. Derewinski, and J.A. Lercher, *Stability of Zeolites in Aqueous Phase Reactions*. *Chemistry of Materials*, 2017. **29**: 7255-7262.

45. Hu, J.Z., C. Wan, A. Vjunov, M. Wang, Z. Zhao, M.Y. Hu, D.M. Camaioni, and J.A. Lercher, *27Al MAS NMR Studies of HBEA Zeolite at Low to High Magnetic Fields*. The Journal of Physical Chemistry C, 2017. **121**: 12849-12854.
46. Vjunov, A., J.L. Fulton, T. Huthwelker, S. Pin, D. Mei, G.K. Schenter, N. Govind, D.M. Camaioni, J.Z. Hu, and J.A. Lercher, *Quantitatively Probing the Al Distribution in Zeolites*. Journal of the American Chemical Society, 2014. **136**: 8296-8306.
47. Holzinger, J., P. Beato, L.F. Lundegaard, and J. Skibsted, *Distribution of Aluminum over the Tetrahedral Sites in ZSM-5 Zeolites and Their Evolution after Steam Treatment*. The Journal of Physical Chemistry C, 2018. **122**: 15595-15613.
48. Persson, A.E., B.J. Schoeman, J. Sterte, and J.E. Otterstedt, *Synthesis of stable suspensions of discrete colloidal zeolite (Na, TPA)ZSM-5 crystals*. Zeolites, 1995. **15**: 611-619.
49. Morales-Pacheco, P., F. Alvarez-Ramirez, P. Del Angel, L. Bucio, and J.M. Domínguez, *Synthesis and Structural Properties of Zeolytic Nanocrystals I. MFI Type Zeolites*. The Journal of Physical Chemistry C, 2007. **111**: 2368-2378.
50. Ding, K., A. Corma, J.A. Maciá-Agulló, J.G. Hu, S. Krämer, P.C. Stair, and G.D. Stucky, *Constructing Hierarchical Porous Zeolites via Kinetic Regulation*. Journal of the American Chemical Society, 2015. **137**: 11238-11241.
51. Verboekend, D., R. Caicedo-Realpe, A. Bonilla, M. Santiago, and J. Pérez-Ramírez, *Properties and Functions of Hierarchical Ferrierite Zeolites Obtained by Sequential Post-Synthesis Treatments*. Chemistry of Materials, 2010. **22**: 4679-4689.
52. Fernandez, C., I. Stan, J.-P. Gilson, K. Thomas, A. Vicente, A. Bonilla, and J. Pérez-Ramírez, *Hierarchical ZSM-5 Zeolites in Shape-Selective Xylene Isomerization: Role of Mesoporosity and Acid Site Speciation*. Chemistry – A European Journal, 2010. **16**: 6224-6233.
53. Wang, Z., Y. Jiang, O. Lafon, J. Trébosc, K. Duk Kim, C. Stampfl, A. Baiker, J.-P. Amoureux, and J. Huang, *Brønsted acid sites based on penta-coordinated aluminum species*. Nature Communications, 2016. **7**: 13820.
54. Coster, D., A.L. Blumenfeld, and J.J. Fripiat, *Lewis Acid Sites and Surface Aluminum in Aluminas and Zeolites: A High-Resolution NMR Study*. The Journal of Physical Chemistry, 1994. **98**: 6201-6211.
55. Omegna, A., J.A. van Bokhoven, and R. Prins, *Flexible Aluminum Coordination in Alumino–Silicates. Structure of Zeolite H–USY and Amorphous Silica–Alumina*. Journal of Physical Chemistry B, 2003. **107**: 8854-8860.
56. Gilson, J.-P., G.C. Edwards, A.W. Peters, K. Rajagopalan, R.F. Wormsbecher, T.G. Roberie, and M.P. Shatlock, *Penta-co-ordinated aluminium in zeolites and aluminosilicates*. Journal of the Chemical Society, Chemical Communications, 1987: 91-92.
57. Chen, J., T. Chen, N. Guan, and J. Wang, *Dealumination process of zeolite omega monitored by 27Al 3QMAS NMR spectroscopy*. Catalysis Today, 2004. **93-95**: 627-630.
58. Pidko, E.A., S.M.T. Almutairi, B. Mezari, P.C.M.M. Magusin, and E.J.M. Hensen, *Chemical Vapor Deposition of Trimethylaluminum on Dealuminated Faujasite Zeolite*. ACS Catalysis, 2013. **3**: 1504-1517.
59. Park, G.T., D. Jo, N.H. Ahn, J. Cho, and S.B. Hong, *Synthesis and Structural Characterization of a CHA-type AlPO<sub>4</sub> Molecular Sieve with Penta-Coordinated Framework Aluminum Atoms*. Inorganic Chemistry, 2017. **56**: 8504-8512.
60. Wang, Z., Y. Jiang, F. Jin, C. Stampfl, M. Hunger, A. Baiker, and J. Huang, *Strongly enhanced acidity and activity of amorphous silica–alumina by formation of pentacoordinated AlV species*. Journal of Catalysis, 2019. **372**: 1-7.
61. Sazama, P., B. Wichterlova, J. Dedecek, Z. Tvaruzkova, Z. Musilova, L. Palumbo, S. Sklenak, and O. Gonsiorova, *FTIR and 27Al MAS NMR analysis of the effect of framework Al- and Si-defects in micro- and micro-mesoporous H-ZSM-5 on conversion of methanol to hydrocarbons*. Microporous and Mesoporous Materials, 2011. **143**: 87-96.

62. Ghorbanpour, A., A. Gumidyala, L.C. Grabow, S.P. Crossley, and J.D. Rimer, *Epitaxial Growth of ZSM-5@Silicalite-1: A Core–Shell Zeolite Designed with Passivated Surface Acidity*. ACS Nano, 2015. **9**: 4006-4016.
63. Grey, C.P. and A.J. Vega, *Determination of the Quadrupole Coupling Constant of the Invisible Aluminum Spins in Zeolite HY with <sup>1</sup>H/<sup>27</sup>Al TRAPDOR NMR*. Journal of the American Chemical Society, 1995. **117**: 8232-8242.
64. Deng, F., Y. Yue, and C. Ye, *<sup>1</sup>H/<sup>27</sup>Al TRAPDOR NMR studies on aluminum species in dealuminated zeolites*. Solid State Nuclear Magnetic Resonance, 1998. **10**: 151-160.
65. Liu, Y., S. Müller, D. Berger, J. Jelic, K. Reuter, M. Tonigold, M. Sanchez-Sanchez, and J.A. Lercher, *Formation Mechanism of the First Carbon–Carbon Bond and the First Olefin in the Methanol Conversion into Hydrocarbons*. Angewandte Chemie, 2016. **128**: 5817-5820.
66. Müller, S., Y. Liu, F.M. Kirchberger, M. Tonigold, M. Sanchez-Sanchez, and J.A. Lercher, *Hydrogen Transfer Pathways during Zeolite Catalyzed Methanol Conversion to Hydrocarbons*. Journal of the American Chemical Society, 2016. **138**: 15994-16003.
67. Wang, C., Y. Chu, J. Xu, Q. Wang, G. Qi, P. Gao, X. Zhou, and F. Deng, *Extra-Framework Aluminum-Assisted Initial C–C Bond Formation in Methanol-to-Olefins Conversion on Zeolite H-ZSM-5*. Angewandte Chemie International Edition, 2018. **57**: 10197-10201.
68. Arora, S.S. and A. Bhan, *The critical role of methanol pressure in controlling its transfer dehydrogenation and the corresponding effect on propylene-to-ethylene ratio during methanol-to-hydrocarbons catalysis on H-ZSM-5*. Journal of Catalysis, 2017. **356**: 300-306.
69. Martinez-Espin, J.S., M. Mortén, T.V.W. Janssens, S. Svelle, P. Beato, and U. Olsbye, *New insights into catalyst deactivation and product distribution of zeolites in the methanol-to-hydrocarbons (MTH) reaction with methanol and dimethyl ether feeds*. Catalysis Science & Technology, 2017. **7**: 2700-2716.
70. Liu, Y., F.M. Kirchberger, S. Müller, M. Eder, M. Tonigold, M. Sanchez-Sanchez, and J.A. Lercher, *Critical role of formaldehyde during methanol conversion to hydrocarbons*. Nature Communications, 2019. **10**: 1462.
71. Hwang, A., M. Kumar, J.D. Rimer, and A. Bhan, *Implications of methanol disproportionation on catalyst lifetime for methanol-to-olefins conversion by HSSZ-13*. Journal of Catalysis, 2017. **346**: 154-160.
72. Khare, R., Z. Liu, Y. Han, and A. Bhan, *A mechanistic basis for the effect of aluminum content on ethene selectivity in methanol-to-hydrocarbons conversion on HZSM-5*. Journal of Catalysis, 2017. **348**: 300-305.
73. Yarulina, I., A.D. Chowdhury, F. Meirer, B.M. Weckhuysen, and J. Gascon, *Recent trends and fundamental insights in the methanol-to-hydrocarbons process*. Nature Catalysis, 2018. **1**: 398-411.
74. Yarulina, I., S. Bailleul, A. Pustovarenko, J.R. Martinez, K.D. Wispelaere, J. Hajek, B.M. Weckhuysen, K. Houben, M. Baldus, V. Van Speybroeck, F. Kapteijn, and J. Gascon, *Suppression of the Aromatic Cycle in Methanol-to-Olefins Reaction over ZSM-5 by Post-Synthetic Modification Using Calcium*. ChemCatChem, 2016. **8**: 3057-3063.

**Table of Contents (TOC) Graphic:**